ROMANIAN JOURNAL OF INFORMATION SCIENCE AND TECHNOLOGY
Volume **10**, Number 1, 2007, 43–52

Ceramic Micro Heater Technology for Gas Sensors

C. MOLDOVAN[1], O. NEDELCU[1], P. JOHANDER[2], I. GOENAGA[3], D. GOMEZ[3], P. PETKOV[4], U. KAUFMANN[5], H.-J. RITZHAUPT-KLEISSL[5], R. DOREY[6], K. PERSSON[7]

[1]National Institute for R&D in Microtechnologies, Erou Iancu Nicolae 32 B, Bucharest 077190, Romania
[2]IVF – Industrial Research and Development Corporation; Argongatan 30, S431 53 Molndal, Sweden
[3]Fundacion Tekniker, Micro and Nanotechnology Department, Av. Otaola 20, 20600 Eibar, Spain
[4]Manufacturing Engineering and Multidisciplinary Technology Centre, Cardiff University, UK
[5]Forschungszentrum Karlsruhe, Institut für Materialforschung III, P.O. Box 3640, 76021 Karlsruhe, Germany
[6]Nanotechnology Group, Cranfield University, Cranfield, Bedfordshire, UK
[7]IMEGO, Arvid Hedvalls Backe 4, SE 411 33 Goteborg, Sweden

Abstract. The paper presents the design and manufacturing steps of micro heaters, built on ceramic suspended membranes for gas sensor applications. The micro heaters are designed and fabricated by combining laser milling techniques, and conductive ceramic technology. Trenches are created in the ceramic substrate in order to define the geometry of the heater using laser processing of the substrate. The heater is completed by filling the trenches with conductive ceramic paste and then baking to remove the solvent from the paste. The final step involves releasing the membrane by laser milling, enabling it to be suspended on four bridges, to minimise the dissipation of the heat in the substrate. The temperature of the heater element was measured with a heat camera from FLIR 40 system comparing the case of the heater positioned on top of a released membrane and that of the non-released membrane. The simulation of the heater build on top of a released membrane was compared with the heater measurements.

Keywords: Micro heaters, gas sensor.

1. Introduction

Micro heaters are an essential part in chemoresistive gas sensors [1]. The heating element must create an accurate and uniform heating of the sensor surface. The heating element is normally made on Silicon, LTCC or alumina substrate. The common methods to manufacture heating element is thin film deposition of metal and lithographic/ etch process [2] and thick film screen printed on LTCC and alumina [3]. The heat distribution in such 2D design concepts is not so good due to the spreading of heat and thus quite large power consumption. This could be improved by a 3D design concept by suspending the heating element in four bridges, so the heating and sensing element will be thermally isolated from the surrounding substrate. This has been demonstrated in silicon by bulk etching of silicon [4], [5]. This design gives a much more uniform heating of the sensor surface and much faster heating characteristics. In this paper we demonstrate a similar design concept by laser machining in LTCC and alumina.

Laser milling process overview

Laser milling involves applying laser energy to remove material through ablation in a layer-by-layer fashion. CNC programs for laser milling are obtained directly from a three-dimensional CAD model of the workpiece. Thus, apart from being a material removal rather than material accretion system, a laser-milling machine operates like any other layered technology manufacturing equipment.

Material removal

The laser milling process removes material as a result of interaction between the laser beam and the substrate or workpiece. Several removal mechanisms can take place, depending on a number of process parameters related to the beam and the workpiece material.

During interaction between the laser radiation and the material, electrons in the substrate are excited by the laser photons. As a result, the electron subsystem is heated to a high temperature and the absorbed energy is transferred to the atomic lattice [6]. Energy losses are caused by heat transport via electrons into the bulk of the substrate. According to classical linear theory, light absorption is described by the Beer-Lambert law, which states that the absorption of a particular wavelength of light transmitted through a material is a function of the material path length and is independent of the incident intensity. For the very high intensities, which can be achieved in laser processing, non-linear phenomena take place and cause stronger energy absorption. According to the linear absorption model, the electrons excited by photon absorption transfer the heat energy to the lattice and cause melting or vaporisation. In the case of extreme intensities, as with ultrashort pulse ablation, the bound electrons of the material can be directly freed. Effects such as multiphoton absorption and avalanche ionisation can be observed. Thermal conduction in the material draws energy away from the focal spot and leads to heat affected zones. For metals, laser

light absorption is not a major problem, because the band structure of the material allows the absorption of most low-to-moderate energy photons. Metals absorb laser radiation with their electrons in the conduction band and near to the Fermi level. For semiconductors and insulators, including ceramics and polymers, the Fermi level is between the valence and conduction bands. The requirement that an electron has to absorb enough energy to pass through the forbidden region between the valence and conduction bands sets a limit on the photon energies that can be absorbed by a linear process. There are two methods for non-linear absorption: an electron avalanche and a strong multiphoton absorption.

In the case of an electron avalanche, some electrons with intermediate energies are excited into the conduction band by single photon absorption. The electrons in the conduction band can absorb single photons of the incident light, which will increase their energy. These electrons collide with bound electrons, which lead to avalanche ionisation.

Multiphoton absorption is another mechanism for non-linear absorption in which an electron transfers from the valence band to the conduction band by absorbing several photons. In general, as materials reach a critical density of electrons, they start to absorb sufficient photon energy to undergo ablation. It is important to note that there is a material dependent ablation threshold fluence, below which the laser ablation cannot start and material removal is not feasible.

The response of the substrate to laser radiation is influenced by a number of material characteristics. Hence, for optimal machining results a proper match of laser source and material should be achieved. Generally, higher absorption efficiency leads to a more effective laser milling process. Thermal conductivity is another key material factor. This affects the dissipation of the absorbed energy into the bulk of the material, the energy losses, the material removal efficiency and the dimensions of the heat affected zone (HAZ) [7], [8].

2. Experimental set up

A commercial femtosecond Ti:sapphire laser system has been used to perform the micromachining of LTCC and briefly, the system is basically composed by:

(i) a femtosecond seed laser (Coherent, Vitesse LP SB) with an output average power of 250 mW at a pulse repetition rate (PRR) of 80 MHz;

(ii) a multipass amplifier (Quantronix, Odin-Compact DP 1.0) based on Chirped Pulse Amplification (CPA);

(iii) a LBO crystal for doubling the natural wavelength of Ti: sapphire beam from $\lambda = 800$ nm to $\lambda = 400$ nm by means of Second Harmonic Generation (SHG) techniques.

The resulting beam, used to perform all the experimental tests presented in this work, is gaussian (beam quality, $M^2 \sim 1.2$ (TEM_{00})), circular (3 mm in diameter), ultraviolet ($\lambda = 400$ nm), pulse length is 90 fs and the maximum energy peak is

350 μJ. Fluence on the sample has been controlled by the rotation of a half-wave plate that changes the polarization plane of the beam before the LBO crystal. Considering that the conversion efficiency strongly depends on the polarization direction, it was possible to control energy variations from 0 μJ to 350 μJ in steps of 1 μJ.

The samples for the experimental tests were placed in a computer controlled XYZ-stage positioning system from Aerotech with resolution of 0.1 μm and repeatability (3σ) of 1 μm in the case of the XY-stages and 0.5 μm and 2 μm, respectively, for the Z-stage. A circular 2 mm mask was used before focusing the beam on the sample in order to remove the tails of the gaussian profile. A fused silica plano-convex lens with focal length of 100 mm (Newport, SPX022) was used as focusing optics. In all cases, focal point was focused on the surface of the sample and no image projection technique was used.

3. Design and manufacturing

The heating element is suspended in four supporting bridges that also serve as electrical leads to the heating elements (see Fig. 1). The two other beams could be used for connection of sensor element. The heating element is a serpentine directly laser-milled into the substrate material and filled with AuPtPd paste. The heater element is released by laser milling and the backside of the heater is thinned so the thermal mass is reduced (Figs. 2 and 3).

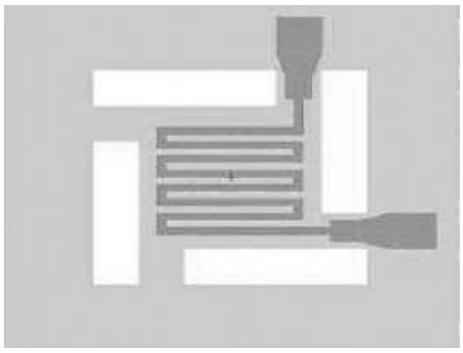

Fig. 1. The design of the electroceramic heater (100 mm width) on the ceramic membrane (2 000×2 000 mm^2) suspended on four bridges (300×200 mm^2 each).

Laser technology has been performed for:

(i) the micromachining of a groove-electrode structure where conductive ceramic paste will be embedded;

(ii) the thin and release of the microheater, driving to a suspended membrane.

In the first case, the laser was slightly de-focussed on the sample in order to get a bigger spot size, leading to a faster machining of the 100 mm-wide grooves. The applied

fluence was 5.5 J/cm^2 at a federate of 0.5 mm/s. The obtained depth was 45 mm. For the electrode contacts, the same parameters were considered. The machining of this elements was performed by means of concentric curves with an offset of 25 mm. Once the heater groove was machined and filled with AuPtPd paste, the next step was to proceed with the thinning and release of the heater. First the releasing operation was performed, that is, the creation of the four bridges around the heater. This operation was completed by going over 0.5×2 mm rectangles several times till the full thickness of the wafer was machined, and consequently a rectangular hole was created. The laser was focused onto the sample through a 100FL lens and the spot size of the focused beam was 36 mm±1 mm. A applied fluence was 1.8 J/cm^2 at a federate of 0.5mm/s Once the releasing step was completed, the thinning of the backside was done. This was performed by "scanning" the 3×3 mm area with the laser as shown in Fig. 4, where the lateral step size (s) was 6 mm. The fluence value used was 3.7 J/cm^2 at the same federate. As a result of the thinning process, a total thickness of 175 microns of material was removed, leaving a membrane of about 225 mm. The same focusing lens and spot size that on the previous step were used for thinning.

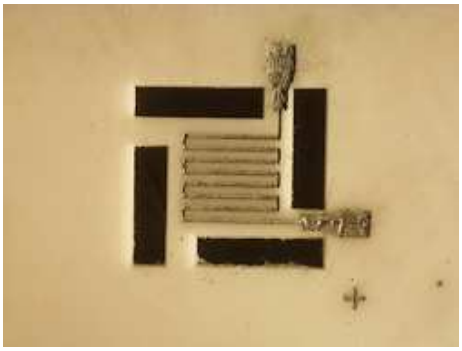

Fig. 2. The suspended heating element.

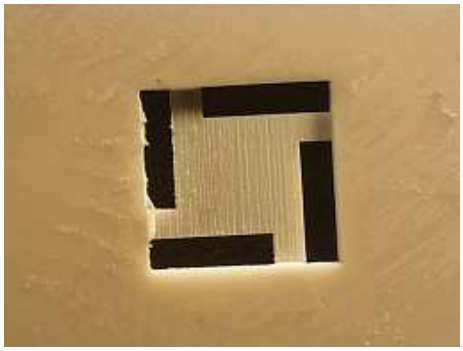

Fig. 3. The heater element from the backside showing the thinning of the substrate.

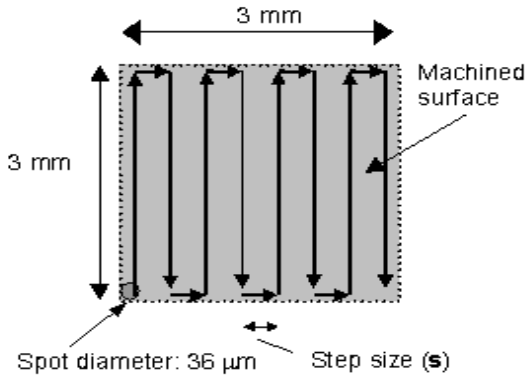

Fig. 4. The laser milling sequence.

4. Measurement of the thermal properties

The temperature of the heater element was measured with a heat camera from FLIR 40 system. This system could record 50 images/s and the dynamics of the system could be analysed. The heater reaches about 490°C in 5 seconds.

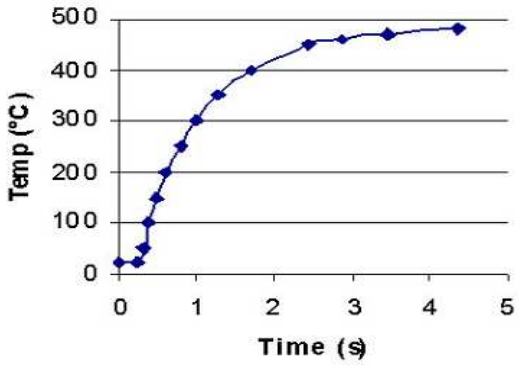

Fig. 5. The power-on curve for the released heater element.

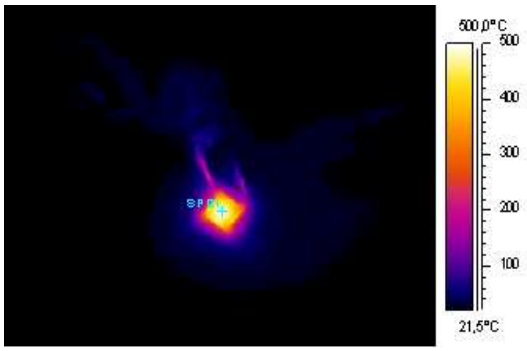

Fig. 6. The heat distribution from the released heating element.

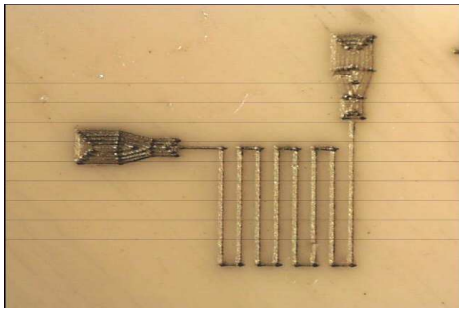

Fig. 7. The Non-released heater element.

This should be compared with non-released heater element in Fig. 8. Because the heat spread in all directions outwards from heater elements we get at circular temperature distribution round the element. In Fig. 6 the temperature is uniform at the released area and the outside area at least 400°C lower temperature. The input power was 1.1 W and this should be compared with the non-released heater element that requires 2.4 W input power of to reach 490°C [1]. The heat distribution around the heater element could be seen in Fig. 8 below.

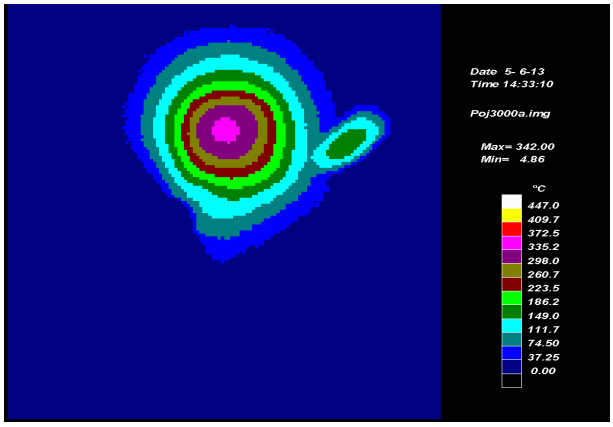

Fig. 8. The heat distribution of a non-released heater element as seen in Fig. 7.

5. Simulation of the thermal behavior of the integrated heater on the ceramic membrane

The simulation of the heat dissipation had the role to validate the chosen design and technology of the sensor. The simulations were made considering the case of the heater positioned on top of the released ceramic membrane. The comparison between the simulation results and measurements results in the conditions of identical layout and technological steps, allows concluding on the heaters processing and efficiency. The simulations have the role to minimize the experiments and to validate the sensor design. The simulations were performed with CoventorWare2004, MemMech module [1].

- Heater material: LTCC AuPdPt paste.
- The simulation conditions: 550°C, Step time: 0.02 sec; Solver step: 0.01 sec; Analyzed time: 0 – 0.2 sec.
- Applied conditions for simulation: a) Constant temperature in heater volume (550°C); b) Initial temperature in ceramic substrate: 293 K; c) Convection through external surfaces: convection coefficient: 25 W/m^2K; ambient temperature: 293 K. The dimensions of the heater are similar to the Mask 1 (Fig. 1). All material constants were considered for the conditions described above.

The results are presented in Figs. 9 and 10 indicating the thermal distribution in the ceramic substrate after 0.02 s (Fig. 9) and after 0.2 s (Fig. 10). A very uniform distribution of the heat after 0.2 s can be observed.

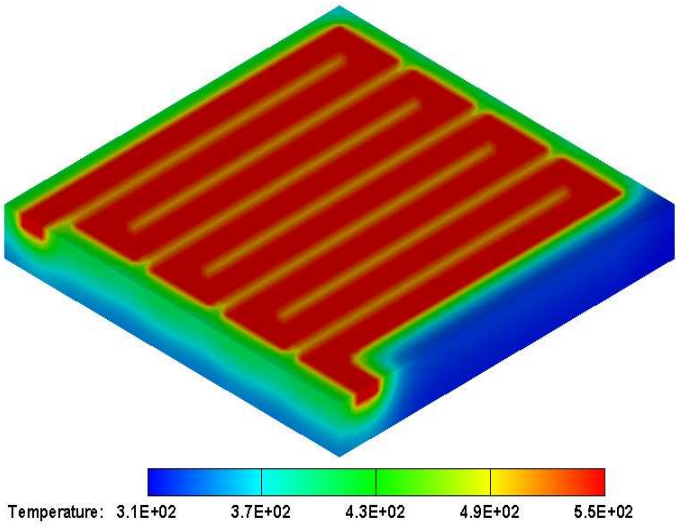

Fig. 9. Thermal distribution after 0.02 s at 550°C.

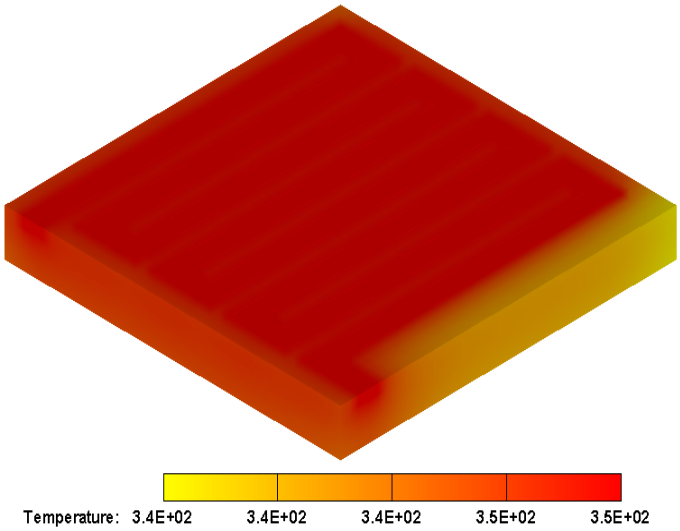

Fig. 10. Thermal distribution after 0.2 s at 550°C.

Figure 11 is describing the evolution of the heating process.

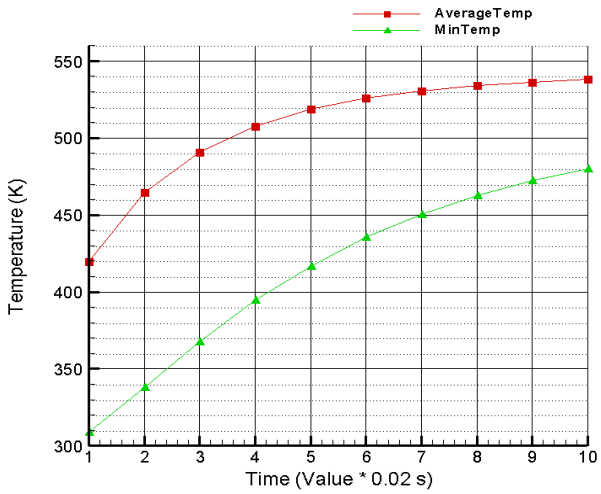

Fig. 11. Evolution of average and minimum temperature in alumina substrate.

Comparing Fig. 10 showing the simulation of the thermal distribution with Fig. 6 showing the measurements of the heat distribution from the released heating element, we can conclude on the similarities of the thermal behaviour in terms of reached temperature (500°C) and area of temperature distribution (identical for both cases, concentrated on the released membrane). The membrane suspended by four microbridges is uniformly heated at 500°C, providing the needed temperature for the working sensor. In the case of measurements, the time for uniformly heating of the membrane depends on the power supply. In the case of simulation, there are no electrical parameters involved in the model, and the model is considering that the substrate will be kept at constant temperature 550°C. That way, the differences appeared between simulation and measurements (Figs. 5 and 11) in terms of the time for uniform heating of the substrate at 500°C can be explained.

6. Conclusions

The purpose of the work was to establish the technology for obtaining heaters allowing the uniform heating of the sensor substrate to be used in gas sensors microfabrication.

The heaters design and manufacturing methodology described in the paper will act as a demonstrator for that technology. The main goal/overall objective is to obtain miniaturized, low cost devices on non-silicon substrates, with high sensitivity and low power consumption to be used in portable devices. The described technologies allow the generation of new type of microsensors with existing tools (software, technological facilities, etc.).

Acknowledgements. The authors express the acknowledgements to the 4M NoE for supporting the work described in this paper. All results have been obtained in the

frame of 4M, WP8 (Ceramic Cluster). Anders Löfgren Ericsson MicroWave for kind helps with the IR measurements.

Literatur

[1] MOLDOVAN, C., NEDELCU, O., KAUFMANN, U., RITZHAUPT-KLEISSL, H.J., DIMOV, S., PETKOV, P., DOREY, R., PERSSON, K., GOMEZ, D., JOHANDER, P., *Proceedings 4M Conference on Multi Material Micro Manufacture*, 29 June – 1 July 2005, Karlsruhe, pp. 211–217.

[2] SHUEHL, J., CAVICCHI, R. E., GAITAN, M., SEMANCIK, S., IEEE Electron Devices Lett., **14**, 1993, pp. 118–120.

[3] ZAWADA, T., DZIEDZIC, A., GOLONKA, L. J., *14^{th} European Microelectronics and Packaging & Exhibition*, Friedrichhafen, Germany, 23–25 June 2003.

[4] SEMANCIK, S., CAVICCHI, R. E., WHEELER, M. C., TIFFANY, J. E., POIRIER, G. E., WALTON, R. M., SUEHLE, J. S., PANCHAPAKESAN, B., DEVOE, D. L., Sensor and Actuators, **B77**, 2001, pp. 579–591.

[5] WELCH, J., *Micro-Machined Thin Film Hydrogen Gas Sensors*, *Proceedings 2002 US DOE Hydrogen Program Review NREL/CP-610-32405*.

[6] SHIRK, M. D., MOLIAN, P. A., *A review of ultrashort pulsed laser ablation of materials*, Journal of Laser Applications, vol. **10**, no. 1, 1998, pp. 18–28.

[7] KAUTEK, W., KRÜGER, J., *Femtosecond pulse laser ablation of metallic, semiconducting, ceramic and biological materials*, *Proceedings SPIE*, vol. **2207**, 1994, pp. 600–610.

[8] VON DER LINDE, D., SOKOLOWSKI-TINTEN, K., *The physical mechanisms of short-pulse laser ablation*, Applied Surface Science, vol. **154**–**155**, 2000, pp. 1–10.